Research Article

In Vitro Chemotaxis and Tissue Remodeling Assays Quantitatively Characterize Foreign Body Reaction

Maren Jannasch [#1], Tobias Weigel [#1], Lisa Engelhardt [1], Judith Wiezoreck [1], Sabine Gaetzner [1], Heike Walles[1,2], Tobias Schmitz [1] and Jan Hansmann[1,2]

[1]University Hospital Wuerzburg, Department of Tissue Engineering and Regenerative Medicine (TERM), Wuerzburg, Germany; [2]Translational Center Wuerzburg "Regenerative Therapies in Oncology and Musculoskeletal Disease" Wuerzburg branch of the Fraunhofer Institut Interfacial Engineering and Biotechnology, Wuerzburg, Germany

Summary

Surgical implantation of a biomaterial triggers foreign-body-induced fibrous encapsulation. Two major mechanisms of this complex physiological process are (I) chemotaxis of fibroblasts from surrounding tissue to the implant region, followed by (II) tissue remodeling. As an alternative to animal studies, we here propose a process-aligned *in vitro* test platform to investigate the material dependency of fibroblast chemotaxis and tissue remodeling mediated by material-resident macrophages.

Embedded in a biomimetic three-dimensional collagen hydrogel, chemotaxis of fibroblasts in the direction of macrophage-material-conditioned cell culture supernatant was analyzed by live cell imaging. A combination of statistical analysis with a complementary parameterized random walk model allowed quantitative and qualitative characterization of the cellular walk process. We thereby identified an increasing macrophage-mediated chemotactic potential ranking of biomaterials from glass over polytetrafluorethylene to titanium. To address long-term effects of biomaterial-resident macrophages on fibroblasts in a three-dimensional microenvironment, we further studied tissue remodeling by applying macrophage-material-conditioned medium on fibrous *in vitro* tissue models. A high correlation of the *in vitro* tissue model to state of the art *in vivo* study data was found. Titanium exhibited a significantly lower tissue remodeling capacity compared to polytetrafluorethylene. With this approach, we identified a material dependency of both chemotaxis and tissue remodeling processes, strengthening knowledge on their specific contribution to the foreign body reaction.

Keywords: foreign body reaction, fibroblast chemotaxis, tissue remodeling, *in vitro*, quantitative characterization

1 Introduction

Tissue injury caused by the surgical implantation of a medical device triggers the release of alarm signals into the extracellular space. These signals stimulate migration of immune cells from the vasculature to the implant region. In a first line of defense, secretory cells like granulocytes and pro-inflammatory M1 macrophages structurally attack the implant surface in an acute inflammatory response by secretion of enzymes and reactive oxygen species. Due to the implant's size and its non-degradable nature, M1 macrophages fail to clear the foreign body by phagocytosis. A transition of short-lived inflammatory cells to a long-vitae M2 macrophage phenotype, which mediates the chronic inflammatory response to biomaterials, is observed (van Loon et al., 2013; Murray et al., 2010). M2 macrophages fuse to form a first cellular layer and isolate the foreign body

# authors contributed equally

Abbreviations

3D, three-dimensional; CM, cyan mean intensity; FBR, foreign body reaction; FCS, fetal calf serum; FGF, fibroblast growth factor; GM-CSF, granulocyte-macrophage colony-stimulating factor; M-CSF, macrophage colony-stimulating factor; PDGF, platelet-derived growth factor; PTFE, polytetrafluoroethylene; g_0, standard gravity; TGF-β1, transforming growth factor β1

Received July 21, 2016;
Accepted October 7, 2016;
Epub October 11, 2016
https://doi.org/10.14573/altex.1610071

from the host tissue. These long-term biomaterial-resident M2 macrophages chronically stimulate the surrounding tissue to form a dense collagenous fibrous capsule, which further isolates the foreign body (Grainger, 2013). The chronic deposition of fibrous tissue in the proximity of the foreign body is determined by (I) fibroblast accumulation either by proliferation or chemotaxis from surrounding tissue as well as (II) fibroblast-mediated increased soft tissue synthesis.

Chemotaxis of fibroblasts to the implant region is mediated by inflammation induced by surgical injury and the foreign body itself. The injury-guided chemotaxis mostly originates from intracellular metabolites and proteins liberated into the intercellular space, or cleavage products of extracellular matrix proteins such as collagen, fibronectin or elastin (Albini et al., 1985; Franz et al., 2011). In contrast to these randomly released proteins, foreign-body-induced cytokine release by macrophages exhibits a material-dependent character (Rodriguez et al., 2009). Platelet-derived growth factor (PDGF) (Shreiber et al., 2001; Heldin and Westermark, 1999; Chen et al., 2015; Seppa et al., 1982), fibroblast growth factor (FGF) (Boilly et al., 2000; Grant et al., 1992) as well as transforming growth factor β1 (TGF-β1) (Grant et al., 1992) are prominent

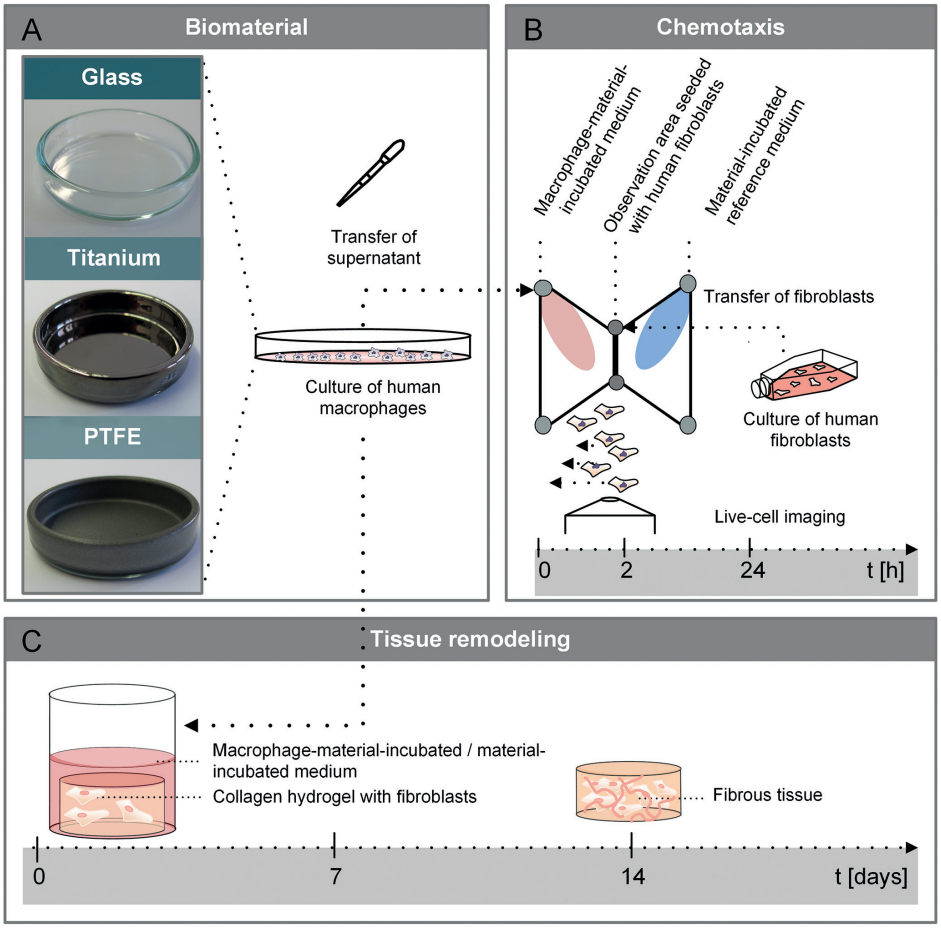

Fig. 1: *In vitro* test platform for evaluating biomaterial-induced fibroblast chemotaxis and tissue remodeling
(A) Human primary M2 macrophages are cultured for 48 h on soda-lime glass, titanium- and PTFE-coated dishes. In response to the biomaterial surface, macrophages are activated to release cytokines into the medium. (B) Two-chamber-based chemotaxis µ-Slides (Ibidi, Martinsried, Germany) allow determination of fibroblast chemotaxis in the direction of macrophage-material-conditioned medium in comparison to material-conditioned control medium. To observe migration along chemokine gradients, fibroblasts in a collagen hydrogel are introduced into the central observation channel. Time-lapse recordings are taken over a period of 48 h in a confocal live cell imaging microscope. Alongside chemotactic effects, macrophage-liberated cytokines elicit long-range chronic activity changes in cells.
(C) Fibroblasts' tendencies to tissue remodeling are evaluated over a 14-day period. Here, human dermal fibroblasts in a three-dimensional (3D) collagen hydrogel are cultured under macrophage-material-conditioned medium. Biomaterial-conditioned medium serves as control medium.

chemokines secreted by macrophages, inducing chemotactic migration of fibroblasts. Ongoing over weeks, fibroblasts in the proximity of the implant encapsulate the foreign body in a chronic matrix remodeling process. Connective tissue remodeling is a balanced process in between fibroblasts' extracellular matrix synthesis and matrix-metalloproteinase-catalyzed matrix degradation (Barron and Wynn, 2011). A key mediator function of TGF-β that shifts this balance towards a higher collagen deposition (Coker et al., 1997) is demonstrated in foreign-body-induced fibrosis (Park et al., 2015) as well as other chronic inflammatory processes like rheumatoid arthritis, intestinal inflammation, diabetic nephropathy or liver fibrosis (Pohlers et al., 2009).

Currently, *in vivo* animal studies represent the gold standard for the assessment of material-induced fibrosis (ISO 10993-6:2007, Part 6; www.iso.org). In contrast to long-term *in vivo* studies, *in vitro* tests facilitate short-term screening for acute effects of blood-material interaction such as coagulation, complement activation or blood cell adhesion (ISO 10993-4:2002, Part 4; www.iso.org). While these models are undoubtedly useful, the specific contribution of chemotaxis and tissue remodeling to the end point of material-induced fibrosis has still not been fully resolved. The identification of sub-processes with a strong material-dependency might facilitate the evaluation and discrimination of biomaterials. Conversely, alignment on sub-processes enables a target mechanism orientated development of materials.

Our experimental approach addresses the processes of (A) acute fibroblast chemotaxis and (B) chronic tissue remodeling to predict macrophage-mediated effects of biomaterials (Fig. 1). To prove the material-dependency of these processes, a standard cell culture glass and two biomaterials, polytetrafluorethylene (PTFE) and titanium, were used. These two biomaterials have a broad range of applications in regenerative medicine: PTFE polymers are used for vascular prosthesis, nerve conduits, or subcutaneous augmentation material (Ahad et al., 2015; Cheesborough et al., 2016), whereas titanium is preferably used in dental and bone replacement (Möller et al., 2012; Souza et al., 2015; Mohammed et al., 2014). In addition to the clinical relevance, the chosen materials exhibit different chemical properties, e.g., distinct water surface interaction from hydrophobic to hydrophilic material characteristics, demonstrated by decreasing water contact angles from 127.1° ±2.8° for PTFE, to 55.0° ±3.3° for titanium, down to 28.8° ±2.7° for glass. Due to the importance of M2 macrophages in the long-term chronic response, a M2-like macrophage phenotype was induced prior to culturing on biomaterial surfaces. To gain a mechanistic understanding of the material-dependency of chemotaxis and tissue remodeling, we examined adsorption and release of the growth factors PDGF, FGF and TGF-β1 into the cell culture supernatant. Material-dependency of chemotaxis was investigated *in vitro* on a micro device consisting of two fluidic reservoirs separated by a central collagen hydrogel channel, which serves as a physiological three-dimensional (3D) scaffold for fibroblasts. The two-chamber design allowed a controlled experimental comparison of (I) macrophage-material-conditioned medium to (II) a standard control medium conditioned with the respective material. By this balanced experimental approach, a prediction of the influence of macrophage-substrate interaction was enabled, and the protein-material adsorption effect was compensated. Statistical analysis in combination with a complementary parameterized random walk model allowed a detailed characterization of fibroblast chemotaxis. To correlate material dependency obtained in chemotaxis, a long-term *in vitro* tissue model consisting of collagen hydrogels with fibroblasts cultured under macrophage-material-conditioned medium, was complemented in our evaluation. These *in vitro* assays render an alternative to animal testing, which bears potential to advance the 3Rs principle by reduction of animal testing in biomaterial research.

2 Methods

Ethical clearance statement

Primary cells were isolated from foreskin biopsies and peripheral blood under informed consent according to ethical approval granted by the institutional ethics committee of the Julius-Maximilians-University Wuerzburg (vote 182/10). Furthermore, procedures were in accordance with the Helsinki Declaration of 1975, as revised in 2008.

Isolation of human dermal fibroblasts

Primary human dermal fibroblasts were isolated from human foreskin biopsies (male healthy donor, 4 years old) according to previously published protocols (Pudlas et al., 2011). DMEM (Gibco, Carlsbad, USA) supplemented with 10% fetal calf serum (FCS) (Gibco) was used to culture fibroblasts. Medium was exchanged every 2 to 3 days. Before setup of a hydrogel or a chemotaxis experiment, fibroblasts were expanded to third passage. To extract the impact of the macrophages, all experiments were performed with one fibroblast donor and the experimental range was expanded by the use of five different macrophage donors.

Isolation and differentiation of human monocytes to macrophages

Mononuclear cells from peripheral blood (anonymized donors, University Hospital Wuerzburg, Germany) were isolated by Ficoll gradient centrifugation (GE Healthcare, Freiburg, Germany). To separate the monocytes from the generated cell fraction, a negative magnetic cell separation was performed by indirectly labeling T cells, NK cells, B cells, dendritic cells, and basophils (Miltenyi Biotec, Bergisch Gladbach, Germany). Obtained monocytes (purity of 90 ± 4%) were cultured in RPMI GlutaMax (Gibco) plus 10% FCS at a concentration of $1*10^6$ cells per ml and a density of $1.5*10^5$ cells/cm^2 on standard polystyrol cell culture dishes (TPP, Trasadingen, Switzerland). Cells were differentiated using 40 ng/ml recombinant human macrophage colony-stimulating factor (M-CSF, Preprotech, New Jersey, United States) for six days (Verreck et al., 2006; Jaguin et al., 2013). Medium was refreshed on the third day. On day six, cells were harvested by PBS plus EDTA incubation on ice for 10 min and followed by mechanical cell

scraping. Before seeding macrophages on test materials, expression of clusters of differentiation was characterized by flow cytometry. The expression profile was evaluated by antibody staining of $2*10^5$ macrophages per antigen. CD14 (555-397, BD Bioscience, Heidelberg, Germany), CD68 (11-0689-42, eBioscience, Frankfurt am Main, Germany), CD163 (12-1639-42, eBioscience), and CD206 (12-2069-42, eBioscience) were used as positive markers for macrophages. Negative markers CD80 (12-1639-42, eBioscience) and CD197 (130-093-621, Miltenyi Biotec), typically expressed by M1 macrophages, were used to guarantee differentiation towards the M2 phenotype. Antibodies were incubated for 30 min at 4°C under light-protection. Isotype controls were used in corresponding concentrations as recommended by the manufacturer. Samples were analyzed in a FACS Calibur flow cytometer (BD Biosciences) and data was further processed in FlowJo software (Tree Star, Ashland, USA).

Preparation of test materials

Titanium films were deposited on glass bowls (30 mm diameter, Brandt, Wertheim, Germany) by radio frequency magnetron sputtering using a titanium target (120 mm diameter, 10 mm height) with a target-to-substrate distance of 100 mm. Glass bowls were cleaned subsequently in ultrasonic baths comprising acetone, isopropanol and ultrapure water, each step taking 10 min, and finally dried by means of nitrogen gas. After evacuation of the process chamber to a base pressure below $1*10^{-6}$ mbar, the sputtering power during deposition was set to 300 W using argon as process gas at a pressure of $3.4*10^{-3}$ mbar with a deposition time of 80 min. PTFE layers (Rhenolase MK I-grau) were prepared by Rhenotherm Kunststoffbeschichtungs GmbH (Kempen, Germany). Prior to a cell test, glass bowls as well as titanium- and PTFE-coated bowls were incubated in an ultrasonic bath with deionized water for 30 min. After a subsequent incubation in 70% ethanol for 15 min, the samples were autoclaved.

Macrophage incubation on material surface and generation of conditioned supernatant

Macrophages were seeded on titanium, glass and PTFE surfaces at a cell density of $3*10^4$ cells per cm^2 at a total medium volume to surface ratio of 0.22 ml per cm^2 in RPMI GlutaMax (Gibco) supplemented with 10% FCS. For comparison of macrophage-biomaterial and medium-biomaterial mediated effects, cell-free RPMI GlutaMax medium supplemented with 10% FCS also was incubated on the material surfaces. All samples were incubated for 48 h at 37°C and 5% CO_2. Medium was harvested after 48 h and centrifuged at $1*10^4$ x g_0 for 5 min to remove any cell fragments. Until use for experiments, supernatants were stored at -20°C. Morphology of macrophages on biomaterial surfaces was demonstrated by immunhistological staining with anti-ICAM-1 antibody (AH55411, Invitrogen, Carsbald, USA) and mounted in Fluoromount plus Dapi (eBioscience).

Cytokine measurement

The secretion of human TGF-β1 (BMS249, eBioscience), FGF (900-K08 Peprotech), and PDGF (900-K04, Peprotech) by macrophages was analyzed according to the manufacturer's protocol by ELISA assays. Each sample was measured in duplicate employing a microplate reader (Tecan Reader infinite® M200, Tecan, Crailsheim, Germany).

Preparation of migration experiment and live cell imaging

Migration experiments were performed according to a previously published protocol (Zengel et al., 2011). In brief, 3 mg/ml rat tail collagen type I (manufactured in-house) in 0.1% acetic acid was equally mixed with neutralization solution, consisting of 20% 10x MEM (Gibco), 150 mM Hepes buffer in water, and adjusted with 1 M NaOH to a final pH of 8.3. Following this, $6*10^6$ fibroblasts per ml DMEM high glucose supplemented with 30% FCS were resuspended in neutralized collagen gel solution in a ratio of one part cell solution to two parts collagen gel. All steps were performed on ice to prevent gelation. The final collagen gel, containing $2*10^6$ fibroblasts in 1x MEM/DMEM medium supplemented with 10% FCS, was filled into the observation channel of a 3D chemotaxis µ-Slide (Ibidi GmbH, Martinsried, Germany). Following gelation for 30 min at 37°C, reservoirs were filled with MEM and DMEM in a 2:1 ratio, comparable to the collagen gel. Each medium was supplemented with 10% FCS. To study chemotaxis, 50% of the medium reservoir was replaced either with (I) chemoattractant TGF-β1 at a final concentration of 12.5 pg/ml as positive control, or (II) macrophage-substrate-conditioned medium. To test for material-medium interactions, the second reservoir was filled with medium conditioned with material in the absence of macrophages. Fibroblast migration was monitored by live cell imaging at 37°C and 5% CO_2 using a confocal laser scanning microscope (TCS SP8, Leica Microsysteme Vertrieb GmbH, Wetzlar, Germany). Images were taken in intervals of 15 min over 48 h.

Trajectory tracking and trajectory discretization

The motion of a cell in a complex microenvironment between initial and final position can be described as a random walk (Kahlig et al., 2013). Hereby, a distinct migration trajectory is specified by a set of n vectors $\{\vec{x}_i\}_{i=1}^{n}$ from the origin to a certain cell position $\vec{x}_i$. Segments defined as straight connections between two consecutive coordinates represent incremental displacements. From each microscopically recorded experiment, trajectories (n = 20) were derived employing the manual tracking plugin of ImageJ (National Institutes of Health, Bethesda, US). Trajectories were stored in text files. The Chemotaxis and Migration Tool (Ibidi) allowed plotting of trajectories.

Calculation of migration velocity and directness, forward migration index and circular statistics

To calculate the migration parameters, trajectory data was imported into MATLAB (The MathWorks GmbH, Ismaning, Germany) and cell positions were transferred to a matrix composed of columns, each representing a trajectory. From this matrix, the dimensionless directness DI can be derived as a measure for a cell's probability to walk in a straight line (Zengel et al., 2011). The Euclidian distance d_E (in µm) and accumulated distance d_A (in µm) of a trajectory are required to determine DI. The d_E

represents the distance between end ($\vec{x}_n$) and start point ($\vec{x}_1$) of a trajectory, whereas the d_A approximates the path integral by

$$d_A = \sum_{i=2}^{n} |\vec{x}_i - \vec{x}_{i-1}|$$

Hereby, $|\ |$ denotes the vector norm. The directness *DI* can be calculated according to

$$DI = \frac{d_E}{d_A}$$

Values for *DI* close to one indicate straight migration. In addition to directness, the efficiency of forward migration in a certain direction represented by a unit vector $\vec{v}$ can be characterized by the dimensionless forward migration index $FMI_{\vec{v}}$ that reads

$$FMI_{\vec{v}} = \frac{\langle \vec{v}, \vec{x}_n - \vec{x}_1 \rangle}{d_A}$$

whereby $\langle\ ,\ \rangle$ is the scalar product.

When supposing that the speed of a migrating cell is independent of migration orientation and only considering the direction of motion in a plane, the travel can be thought of as a random walk on the unit circle specified by a set of *n-1* angles $\{\alpha_i\}_{i=1}^{n-1}$. The turning angle $\Delta\alpha$ was calculated from a matrix composed of columns representing trajectories of a live cell imaging experiment. If a preferred direction of travel is found, the random walk is biased. Circular statistics support analysis of a random walk, e.g., by identification of the angular variance (Hill and Häder, 1997). The circular mean $\tilde{\alpha}$ and the dimensionless mean length *R* are derived from

$$R\ cos(\tilde{\alpha}) = \sum_{i=1}^{n-1} \frac{cos(\alpha_i)}{n-1}, R\ sin(\tilde{\alpha}) = \sum_{i=1}^{n-1} \frac{sin(\alpha_i)}{n-1}$$

When *R* tends to one, the angle distribution is sharply peaked, whereas an almost uniform angle distribution is found for *R* close to zero (Mardia, 1972).

Demonstration of Markow property and estimation of the Kramers-Moyal coefficients

The directness *DI*, the forward migration index $FMI_{\vec{v}}$, the circular mean $\tilde{\alpha}$, and the dimensionless mean length *R* provide statistical characteristics of cell migration. However, they do not provide insight into migration dynamics. Such information can be generated by using a continuous model of cell migration that is parameterized based on experimental data. A basis for a continuous random walk model for the traveling orientation $\alpha(t)$ is constituted by the Fokker-Planck equation

$$\frac{\partial}{\partial t} P(\alpha, t) = \left(-\frac{\partial}{\partial \alpha} D_1(\alpha, t) + \frac{\partial^2}{\partial \alpha^2} D_2(\alpha, t) \right) P(\alpha, t)$$

which has been used previously to investigate moving microorganisms and endothelial cells (Hill and Häder, 1997; Kahlig et al., 2013). A prerequisite for the application of the Fokker-Planck equation is the demonstration that the studied system is memory-free and represents a Markow process (Risken, 2012), which can be achieved using the Chapman-Kolmogorov equation and X^2-statistics (Friedrich et al., 2000). Markow property was verified by X^2-statistics for different time steps Δt. Therefore, the conditional probability density $P(\alpha+\Delta\alpha, t+\Delta t \mid \alpha, t)$ for the turning angle $\Delta\alpha$ was calculated and continuity properties were ensured. The conditional probability density was processed using a moving average. Two consecutive positions of a defined time difference Δt were identified and, based on the resulting difference vector, the probability for a distinct turning angle $\Delta\alpha$ was derived along the trajectories. Hereby, Δt was a multiple integer of the sampling rate. The numerical evaluation of

$$X^2 = \int_{\Omega} \int_{\Omega} \frac{\left(P(\alpha + \Delta\alpha, t + \Delta t | \alpha, t) - \tilde{P}(\alpha + \Delta\alpha, t + \Delta t | \alpha, t) \right)^2}{P(\alpha + \Delta\alpha, t + \Delta t | \alpha, t) + \tilde{P}(\alpha + \Delta\alpha, t + \Delta t | \alpha, t)}\ d\alpha\ d\Delta\alpha$$

allowed identifying a suitable time step for which the Markow assumption held. Markow property was assumed for a significance level exhibiting a probability of 95%.

In the Fokker-Planck equation, the so called Kramers-Moyal coefficients $D_1(\alpha,t)$ and $D_2(\alpha,t)$ describe drift (D_1) and diffusion (D_2) of the probability distribution. When supposing a small constant time shift Δt between all changes in orientation, migration direction is either changed by a small angle $\Delta\alpha(t)$ or remains. From the conditional probability density $P(\alpha+\Delta\alpha, t+\Delta t \mid \alpha, t)$ of distinct time steps, the Kramers-Moyal coefficients can be calculated by

$$D_n(\alpha, t) = \frac{1}{n!} \lim_{\Delta t \to 0} \frac{1}{\tau} \int_{\Omega} \Delta\alpha^n\ P(\alpha + \Delta\alpha, t + \Delta t | \alpha, t)\ d\Delta\alpha$$

to parameterize the respective random walk model (van Mourik et al., 2006). The parameterized model allows analyzing system dynamics and identification of migration stability and robustness.

Macrophage-conditioned culture of human dermal fibroblasts in a collagen hydrogel

Long-term effects of macrophage-conditioned medium on fibroblasts in a collagen hydrogel were studied to assess tissue remodeling. Fibroblasts were suspended in 500 µl rat tail collagen type I hydrogel (manufactured in-house) at a final concentration of $2*10^5$ cells per ml. Following gelation for 30 min at 37°C, hydrogels were overlayered with 250 µl medium: (I) 1 ng/ml TGF β1-enriched (Peprotech) medium, or (II) standard DMEM high glucose medium supplemented with 10% FCS, or (III) 30% macrophage-material-conditioned medium, or (IV) 30% cell-free material-conditioned medium. All medium approaches were supplemented with 100 µM ascorbic acid phosphate (Wako, Neuss, Germany) to support collagen synthesis. Experiments were performed in triplicate for each macrophage donor. Medium was exchanged every second to third day. On day 14, wet weight was measured and samples were fixed in 4% paraformaldehyde over night at 4°C followed by paraffin embedding. Tissue sections of 5 µm thickness were stained for connective tissue with Azan staining according to the manufacturer's protocol (Morphisto, Frankfurt, Germany).

Image analysis

Images of tissue sections were taken with fluorescence microscope BZ-9000 (Keyence, Neu-Isenburg, Germany). Further

analysis was performed using ImageJ software. Background subtraction was equally performed on all images, using the rolling ball method with a diameter of 3000 pixels. Azan staining allowed a qualitative evaluation of collagen tissue remodeling of histological images. To quantify tissue remodeling, the cyan mean intensity (CMI) was analyzed. Histological images were decomposed to CMYK-images to evaluate the CMI value. Following this, cyan channel images were converted to 8-bit. Histograms enabled the read-out of the CMI for Azan-stained histological sections.

Statistical analysis

Continuous donor-dependent data was analyzed for normal distribution using the Shapiro-Wilk test. If normal distribution was confirmed, statistical differences were analyzed using one-way repeated measures ANOVA, followed by a post-hoc Fisher's least significant difference test. For not normally distributed data, Friedman's ANOVA was applied, followed by the Wilcoxon signed rank test to test pair-wise on significant differences. For all statistical tests $p \leq 0.05$ was considered significant.

3 Results

3.1 Characterization of pre-differentiated macrophages

The choice of maturation factors, i.e., granulocyte macrophage colony-stimulating factor (GM-CSF) or macrophage colony-stimulating factor (M-CSF) for macrophage differentiation determines the state of pro- or anti-inflammation of the mature macrophages generated (Vogel et al., 2014). In this study, differentiation to a moderate anti-inflammatory M2 macrophage subtype involved in long-term chronic tissue-remodeling and fibrosis was preferred (Franz et al., 2011). Thus, monocytes were incubated with M-CSF for six days in culture medium (Ambarus et al., 2012; Spiller et al., 2014; Vogel et al., 2014). Robustness of differentiation was confirmed by analyzing phenotypic clusters of differentiation in flow cytometry (Tab. 1). CD14, expected on monocytes as well as on macrophages, was expressed. During macrophage differentiation, the typically upregulated clusters CD68 and CD206 were exhibited by macrophages, and the M2-phenotypic expression of CD163 was shown. The absence of CD80 and CD197, both expressed by M1-phenotypes, verified induced M2 cell identity. Post differentiation, macrophages were cultured on biomaterial surfaces for 48 h. Cellular adherence on biomaterial surfaces was shown by immunhistological staining of ICAM-1 (Fig. 2A).

3.2 Chemokine adsorption on biomaterials and active secretion by biomaterial-resident macrophages

Protein adsorption on biomaterials represents a primary effect of contact of a foreign body with body fluids like blood plasma or interstitial fluid. In our experimental approach, serum supplemented to culture medium naturally contains proteins like growth factors. The supplementation of serum allows mimicking of the first contact of the biomaterial with body fluids. To evaluate the biomaterial-dependency of protein-surface-adsorption, PDGF (Fig. 2B), FGF (Fig. 2C), and TGF-β1 (Fig. 2D) concentrations in biomaterial-conditioned medium in the absence of cells were analyzed. Differences in protein adsorption were revealed among glass, PTFE, and titanium surfaces. Absorption of PDGF and FGF decreased from glass with a high adsorption to PTFE with a moderate adsorption and titanium with the lowest adsorption capacity. Adsorption of TGF-β1 was comparable for glass and PTFE, whereas titanium resulted in the lowest adsorption. These findings indicated that the macrophage-material-modulated contribution to fibroblast chemotaxis and tissue remodeling would have to be compared with medium conditioned with the material in the absence of macrophages. Therefore, material-conditioned medium was used as a control in the two-chamber-based chemotaxis device, opposing chamber was filled with macrophage-material-conditioned medium. Also, in the experimental approach of tissue remodeling, a material-conditioned medium control was included to discriminate between macrophage-surface and medium-surface effects.

In comparison to respective material-conditioned medium in the absence of cells, macrophages cultured on glass surfaces did not significantly modulate PDGF, FGF, and TGF-β1 levels in the medium. Culture on PTFE induced the secretion of PDGF,

Tab. 1: Characteristic expression of M2-phenotypic clusters of differentiation after differentiation of monocytes with M-CSF
The percentage of positively stained clusters of differentiation (CD) on macrophages is shown for five primary cell donors.

Donor no.	Cluster of differentiation (% positive)					
	CD14	CD68	CD80	CD163	CD197	CD206
1	98.6	98.1	0.0	92.8	0.0	88.5
2	98.7	99.0	0.0	88.2	0.0	89.8
3	99.4	89.8	0.0	97.9	0.0	93.7
4	98.8	89.4	0.0	95.2	0.0	95.5
5	97.7	75.1	0.0	91.2	0.0	82.7
Mean	**98.6**	**90.3**	**0.0**	**93.1**	**0.0**	**90.0**
SD	**0.6**	**9.6**	**0.0**	**3.7**	**0.0**	**5.0**

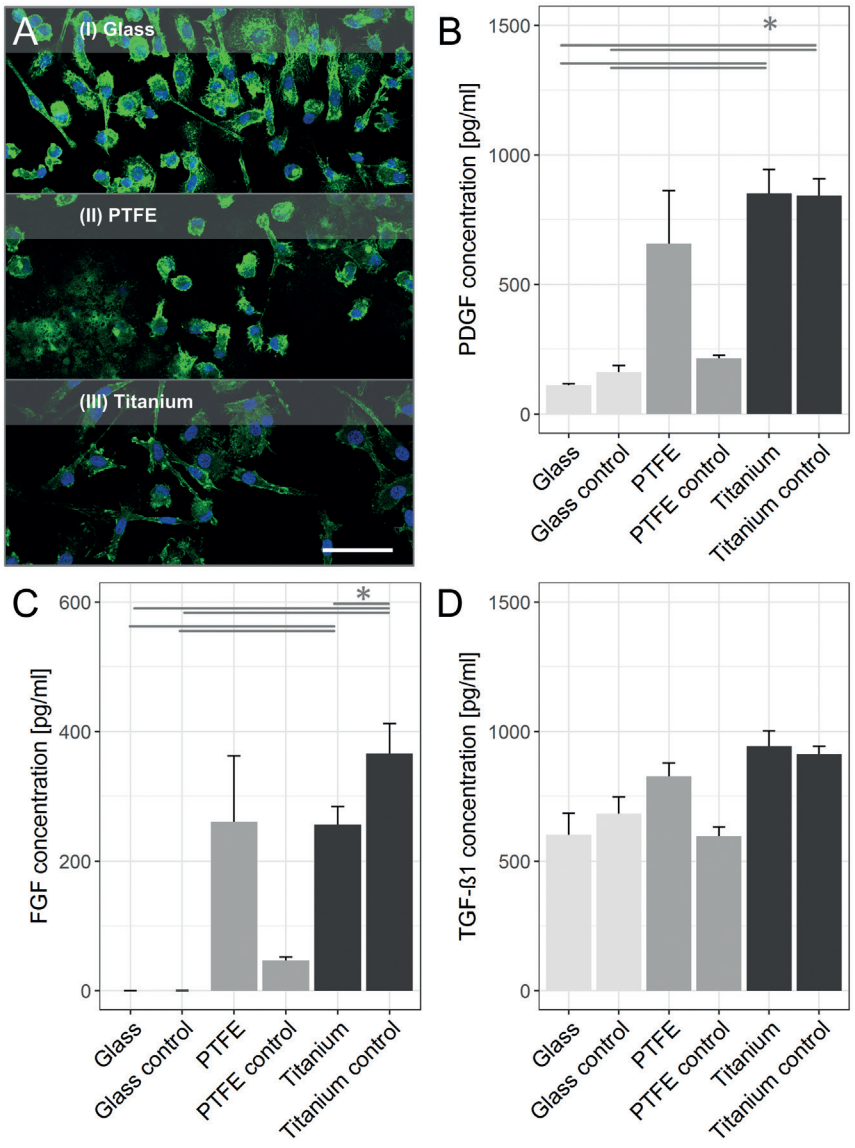

Fig. 2: Macrophage adhesion on biomaterial surfaces, active secretion of growth factors by macrophages, and passive growth factor surface adsorption

Macrophages show a material-dependent adherence on glass, PTFE, and titanium surfaces. (A) Immunhistological staining of intercellular adhesion molecule 1 (ICAM-1, green) and nuclear DAPI staining (blue) visualized macrophage adhesion and morphology on biomaterial surfaces after 48 h. The scale bar indicates 50 µm and is valid for all images. Material-induced active growth factor secretion by macrophages and passive growth factor adsorption on the biomaterial surface were characterized by measurement of (B) PDGF, (C) FGF, and (D) TGF-β1 in macrophage-material and material-conditioned control medium. The PTFE values showed an inhomogeneous variance as well as a not-normally distributed range (p-value > 0.05). Therefore, PTFE values were excluded from the statistical analysis. One-way repeated measures ANOVA on PTFE-excluded datasets showed significant differences between glass and titanium for PDGF and FGF (p-value ≤ 0.05). No significant differences were found for TGF-β1 (p-value = 0.17). A p-value ≤ 0.05 was considered significant. In total, supernatants of five donors were characterized. Mean values ± SEM are represented.

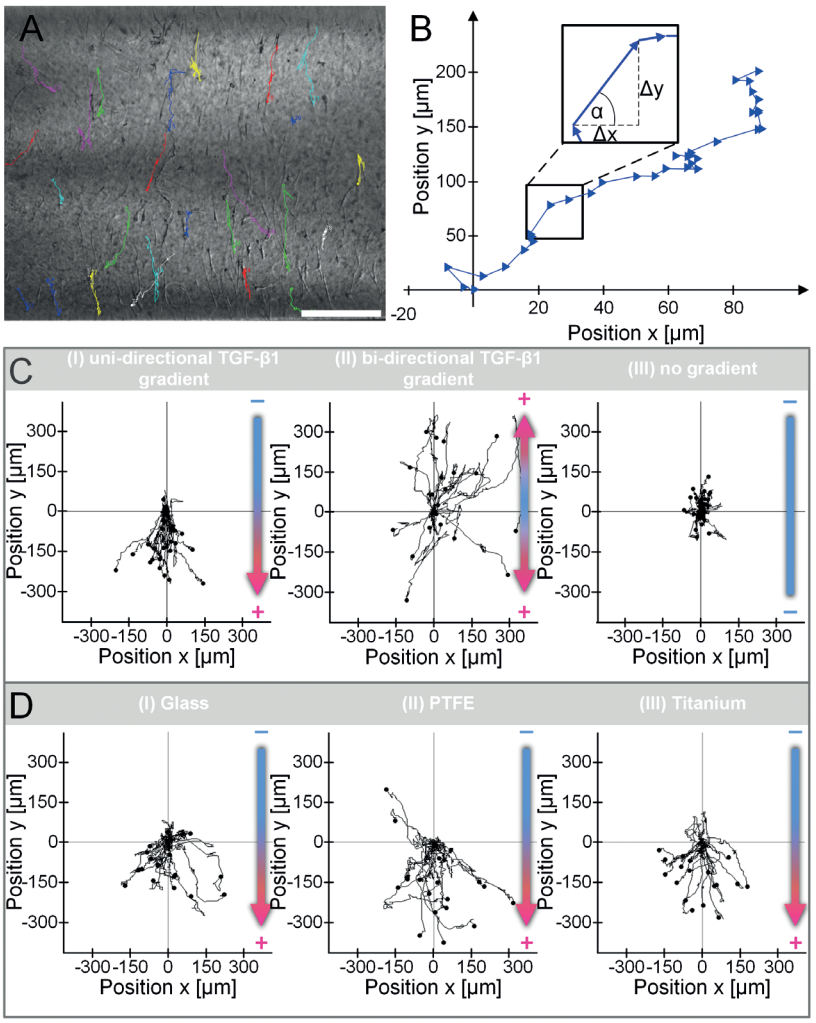

Fig. 3: Tracking and analysis of fibroblast chemotaxis
(A) Trajectories of collagen-embedded fibroblasts in the observation channel were obtained employing live cell imaging microscopy. Each colored line represents a trajectory of an individual cell. The scale bar indicates 250 µm. (B) Recorded trajectories were composed of incremental displacements in the direction that is defined by the angle α (rad). (C) To compare fibroblast chemotaxis, trajectories were displaced so that each walk starts in zero origin. A (I) unidirectional gradient of TGF-β1 resulted in trajectories orientated along the gradient. In contrast, no biased walk was detected for a (II) bi-directional gradient or for (III) fibroblast migration without a gradient. (D) Trajectories recorded from fibroblasts in response to gradients of macrophage-material-conditioned medium. Macrophages cultured on (I) glass, (II) PTFE, or (III) titanium induced fibroblast chemotaxis in the direction of the gradient. Each data set is composed of 20 individual cells. Graphs are exemplarily shown for the supernatant of one macrophage donor.

FGF and TGF-β1 in macrophages. PDGF concentrations increased from 214.4 ±12.7 to 656.4 ±205.7 pg/ml, FGF concentrations increased from 46.7 ±5.4 to 261.0 ±101.2 pg/ml, and TGF-β1 concentrations increased from 596.6 ±36.0 pg/ml to 827.1 ±51.0 pg/ml in PTFE macrophage-conditioned medium. While titanium-resident macrophages did not induce a change of PDGF and TGF-β1 levels, a significant decrease of FGF concentration, from 366.4 ±46.1 pg/ml in material-conditioned blank medium to 256.0 ±28.2 pg/ml conditioned medium, was measured (p-value ≤ 0.05).

3.3 Validation of the experimental chemotaxis design

Employing live cell imaging, trajectories of fibroblasts in a 3D microenvironment were recorded (Fig. 3A). Direction and length of incremental steps were derived from the coordinates (Fig. 3B). To validate the experimental approach in 3D chemotaxis µ-Slides, fibroblast migration towards a defined chemokine gradient of TGF-β1 in (I) uni- or (II) bi-direction was measured and compared to (III) a negative control without any chemical gradient (Fig. 3C). Towards a uni- or bidirectional chemical gradient of TGF-β1, fibroblasts migrated along the gradients. In contrast to a migration towards a unidirectional gradient, the mean direction of migration in between all trajectories was not biased for a bi-directional gradient or migration without gradient. Compared to the cellular walk distance in y-direction without any gradient, the distance between initial and final fibroblasts' position increased for uni- and bi-directional gradient from 150 µm for the negative control to 300 µm in the gradient setup.

In live cell experiments, macrophage-material-conditioned medium induced biased fibroblast migration (Fig. 3D). For all tested materials, fibroblasts aligned their tracks along the gra-

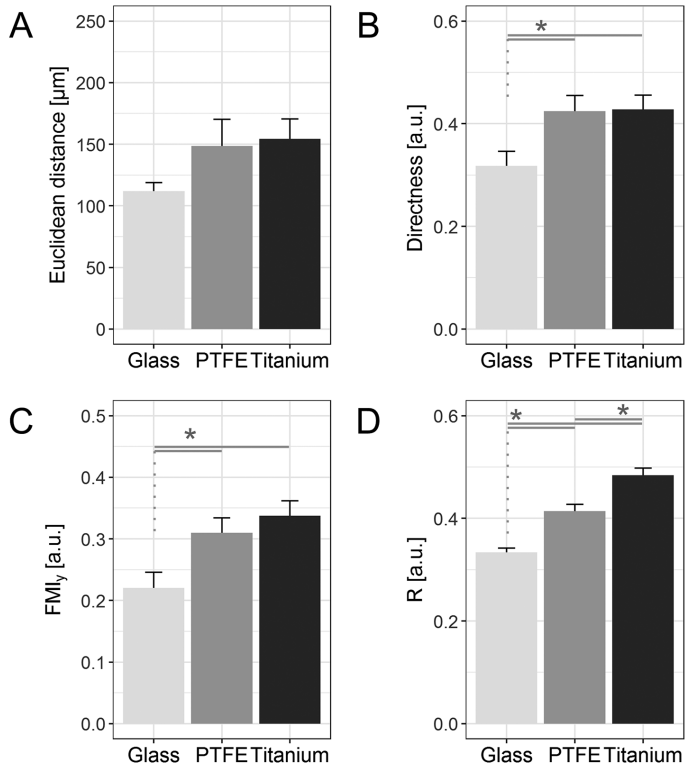

Fig. 4: Statistical analysis of fibroblast chemotaxis
Statistical parameters were derived from recorded migration data.
(A) The difference between initial and end position of a cell is expressed as the Euclidean distance d_E. No significant differences among materials were obtained for d_E.
(B) The directness *DI*, denoted by the quotient between d_E and the accumulated distance d_A, represents a measure for the straightness of the trajectories.
(C) The efficiency of migration in *y* direction can be assessed by the forward migration index (FMI_y).
(D) The mean length *R* provides information on the angle distribution of a migration process. Significant differences between materials were found for *DI*, FMI_y and *R* (p-value ≤ 0.05). Trajectories were analyzed for five primary macrophage donors. Values for each donor are visualized by grey squares. Mean and SEM are shown.

dient. To characterize fibroblast chemotaxis, discretized tracks were analyzed employing linear and circular statistics (Fig. 4). No significant differences were detected for the Euclidian distance d_E. Measured travel distances ranged from 112.0 ±7.0 µm for glass to 154.4 ±16.2 µm for titanium. For the directness D_I, significant differences were found between glass (0.32 ±0.03) and titanium (0.43 ±0.03) as well as glass and PTFE (0.42 ±0.03). The same pattern of significance was revealed for the efficiency of migration in y direction, described by the forward migration index (FMI_y). Here, glass resulted in a FMI_y of 0.22 ±0.03, whereas titanium and PTFE exhibited significantly higher values of 0.34 ±0.02 and 0.31 ±0.02, respectively. For the angle distribution, significant differences were detected between all materials. Highest values for the mean length *R* measured for titanium (0.48 ±0.01) indicated a strongly peaked angle distribution compared to glass (0.33 ±0.01) and PTFE (0.41 ±0.01).

3.4 Dynamics of macrophage-stimulated fibroblast chemotaxis

Linear and circular statistics confirmed the impact of a biomaterial on macrophage-modulated fibroblast chemotaxis. To investigate migration dynamics and migration robustness, a stochastic computational model was developed (Fig. 5). Based on the Fokker-Planck equation, the dynamics of the angle probability distribution were analyzed. Following verification of the Markow property to ensure that the requirements for the applicability of the Fokker-Planck equation are met, Kramers-Moyal coefficients were derived. To calculate $D_1(\alpha,t)$, which represents the biased chemotaxis, and $D_2(\alpha,t)$, which values the unbiased random walk, steady-state conditions were assumed and $D_n(\alpha,t)$ was substituted for $D_n(\alpha)$ (n = 1, 2). For all materials, a zero-crossing embedded in a linear range of $D_1(\alpha)$ was found in the gradient direction (≈ 4.7 rad). The zero

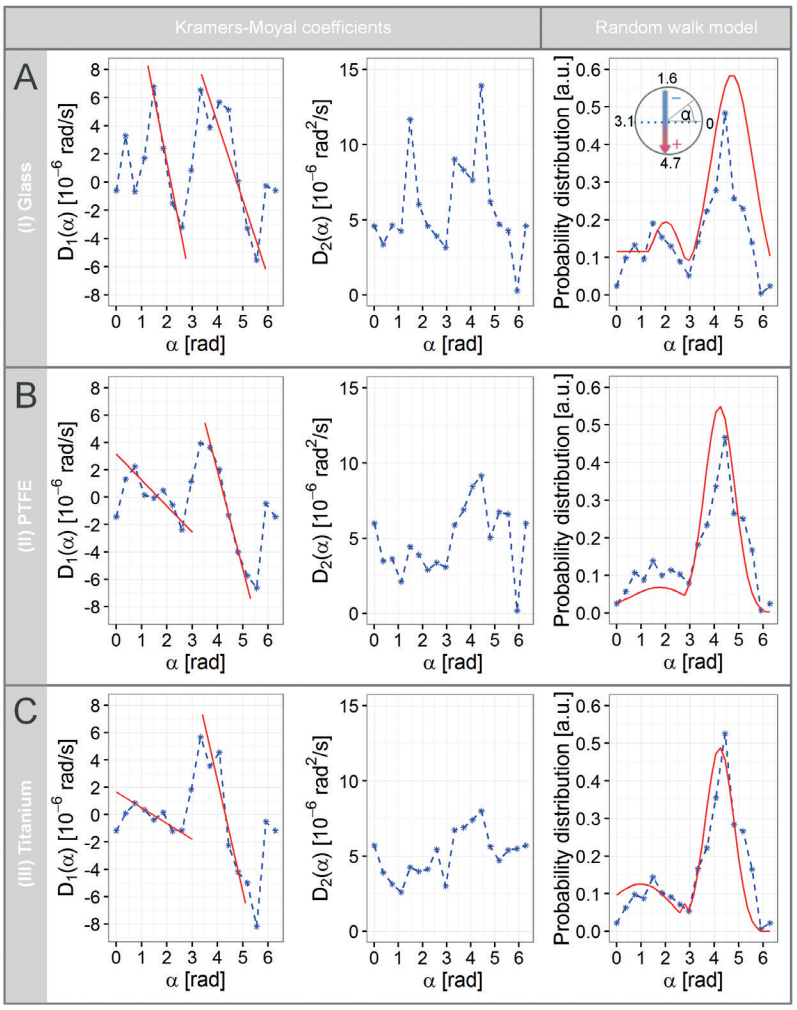

Fig. 5: Continuous random walk model and migration robustness
For all tested materials (A) glass, (B) PTFE, and (C) titanium, the Kramers-Moyal coefficients $D_1(\alpha)$ and $D_2(\alpha)$ were derived. The drift coefficient $D_1(\alpha)$ was characterized by two linear ranges (red lines) with zero points at 1.5 and 4.3 rad. They illustrate a pole in direction (4.3 rad) and an antipole (1.5 rad) in the opposite direction of the chemical gradient. The highest values for diffusion coefficient $D_2(\alpha)$ were detected in the proximity of the zero point. Comparison of measured angle probability distribution (dotted blue line) and the solution of the parameterized Fokker-Planck equation (red line) demonstrated a high predictive power of the stochastic model. For the calculation of the Kramers-Moyal coefficients, 20 tracks of all five donors were compiled (n = 100).

crossing of the drift coefficient accumulates the probability that a cell migrates with a distinct angle, and thus induces a biased walk. Traveling cells are redirected towards the gradient when entering the linear range. Positive deviations between the actual direction and the zero-crossing result in negative drift values, and negative deviations in positive drift values. The width of the linear range determines the region from which cells are guided towards the gradient, and thus the attractivity of the gradient. The slope of the linear range is a measure for the velocity of the reorientation. A second, differently strong pronounced zero crossing of $D_1(\alpha)$ was detected in the opposite direction (≈ 1.5 rad). This antipole weakens the attractivity of the gradient. In addition to biochemical signals, the second zero-crossing is also influenced by event-triggered reorientation, e.g., cell division or cell-cell interaction. Stochastic variations in the migration direction are introduced by the diffusion coefficient. Diffusion in gradient direction was differently increased for the three materials. For glass, the diffusion coefficient as well as the antipole were most pronounced, confirming the lowest induction of fibroblast chemotaxis (Fig. 5A). In contrast, the high chemotactic potential of titanium was reflected by lowest values for the diffusion coefficient and a weakly expressed antipole (Fig. 5C). Induction of fibroblast migration by PTFE is ranked between the other tested biomaterials, depicted by a moderate slope and width of the linear range in addition to values for the diffusion coefficient in between the values of glass and titanium (Fig. 5B). The results of the continuous model provide a qualitative characterization of the migration; nevertheless, obtained findings correspond with the statistical analysis of the recorded trajectories. When substituting the Kramers-Moyal coefficients into the Fokker-Planck equation, the partial differential equation could be solved. Therefore, Kramers-Moyal coefficients were approximated by partial continuous functions. Obtained angle probability distributions correlated with the experimental angle distribution probability patterns, emphasizing the predictive power of the *in silico* model. Thus, the model represents a tool for the generation of mechanistic understanding of fibroblast chemotaxis.

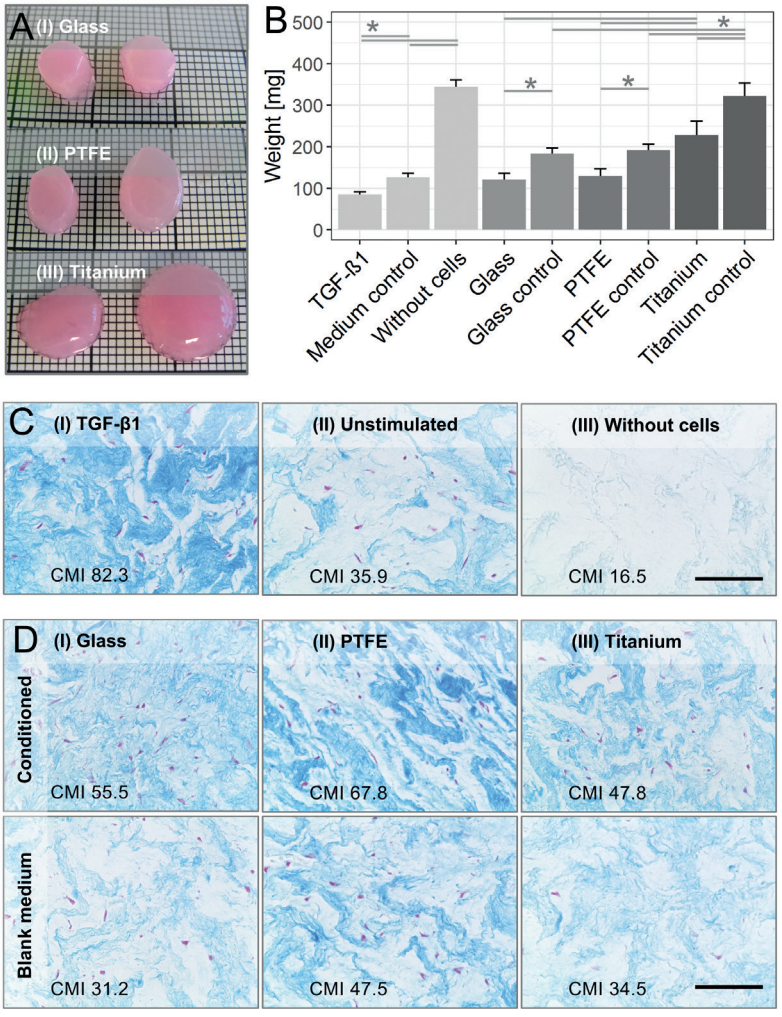

Fig. 6: Fibrous 3D tissue model to evaluate macrophage-material-induced effects on tissue remodeling

Medium conditioned with different materials (glass, PTFE and titanium) and macrophages derived from five human donors were harvested. Samples were each applied to three individual tissue models of fibroblasts in a collagen hydrogel. Respective material-conditioned control medium was used to identify macrophage-specific effects.

(A) On day 14 of culture, macrophage-material-induced effects on hydrogel (left side) contraction compared to the effects of respective material-conditioned control medium (right side) were visually apparent and correlated with the wet weight of tissue samples (B). In the plot, the weight is visualized as mean ± SEM; $p \leq 0.05$ was considered significant. In (C) and (D), tissue remodeling is confirmed by histological Azan staining of fibrous tissue sections. Collagenous fibers appear blue and cell nuclei in purple. Cyan Mean Intensity (CMI) allowed a quantitative evaluation of blue values. Each scale bar represents 100 µm and is valid for all horizontal aligned images.

3.5 Macrophage-mediated tissue remodeling

To confirm the collagen hydrogel concept as a model for *in vitro* tissue remodeling, (I) TGF-β1 was supplemented as a positive control to a 14-day culture of fibroblasts and compared to (II) a hydrogel without additional pro-fibrotic stimulation as well as (III) a hydrogel without cells. For the evaluation of macrophage-biomaterial mediated effects, (IV) macrophage-material conditioned as well as (V) material-conditioned medium were incubated for 14 days on respective fibroblast-based tissue models. Hydrogel contraction was macroscopically visible in all experimental conditions, exemplarily illustrated for the tested materials in Figure 6A.

Tissue remodeling activity of fibroblasts cultured in a collagen hydrogel treated with TGF-β1 or macrophage-conditioned medium compared to cell-free hydrogels, was further demonstrated by a significantly decreased weight (Fig. 6B). For all materials tested, macrophage-material-conditioned medium induced a significant weight reduction of collagen hydrogels in comparison to material-conditioned medium control. This relative weight reduction revealed a material dependent tissue-remodeling effect increasing from glass (weight reduction of 60 mg) to PTFE (weight reduction of 70 mg) and titanium (weight reduction of 90 mg). Related to an initial expected weight of 500 mg, the final weight induced by material-conditioned medium identified a significantly lower weight loss of titanium-conditioned medium (320 ±31 mg) compared to glass-conditioned medium (180 ±13 mg) and PTFE-conditioned medium (190 ±15 mg). Similar patterns of significance were observed between absolute weights under macrophage-material-conditioned medium harvested from titanium (230 ±34 mg) compared to glass (120 ±15 mg) and PTFE (130 ±18 mg).

Observations in weight measurements were confirmed by histological Azan staining of tissue sections. The Cyan Mean Intensity (CMI) value supported qualitative visible histological differences and allowed quantitative evaluation. Proof of collagen hydrogel concept as a model for *in vitro* tissue remodeling was demonstrated by an increased collagen fiber density under TGF-β1-stimulated fibroblast culture (Fig. 6C). The CMI in-

creased from 35.9 without any additional stimulation to 82.3 in the TGF-β1-stimulated tissue. Hydrogels without any cells consisted of loosely structured collagen fibers (CMI 16.5). In comparison to material-conditioned blank medium, macrophage-material-conditioned medium increased collagen fiber density (Fig. 6D). The relative increase of CMI showed a material dependent ranking from titanium (ΔCMI 13.3), to PTFE (ΔCMI 20.3), up to glass (ΔCMI 24.3). Absolute CMI values induced by macrophage-conditioned medium showed a CMI of 47.8 for titanium and 55.5 for glass. The strongest effect was observed on PTFE-conditioned macrophage-conditioned medium. Here, collagen fibers formed concentrated collagen bundles in hydrogels. These effects were reinforced by a relatively high CMI of 67.8.

4 Discussion

In vitro tests are useful to screen medical devices or implants as an alternative to animal studies. One advantage of *in vitro* tests is the avoidance of physiological differences between species by isolation of cells from human tissue, which are subsequently embedded in a biomimetic 3D test microenvironment. Furthermore, *in vitro* tests facilitate the breakdown of complex mechanisms into separate sub-processes, allowing a more precise and detailed study than is possible *in vivo* (ISO 10993-4:2002, Part 4, www.iso.org). In our study, we investigated the material dependency of two sub-processes involved in the foreign body reaction: (A) acute fibroblast chemotaxis, mediated by material-resident macrophages, and (B) chronic modulation of tissue remodeling. The proposed assays provide a new screening platform to ascertain the impact of each process on the apparent grade of foreign body reaction.

A micro device was employed to record real-time single-cell migration, supporting investigations on chemotaxis in a biomimetic microenvironment with well-defined and long-term-stable chemical gradients. Trajectory appearance and directly-accessible migration parameters, such as the Euclidian distance, did not allow to distinguish between different biomaterials. Material differentiation was achieved by employing linear and circular statistics, whereby the analysis of the migration angle resolved the materials' chemotactic capacity most distinctively. Due to these findings, a biased random walk model for the migration angle was developed. Such continuous models enable unraveling complex empirical data (van Mourik et al., 2006). The investigated model parameters allowed assessing the biomaterials' potential to induce fibroblast migration. Zero crossings of the drift coefficient determine the preferred migration direction. The derived model parameters allow a scoring of the tested biomaterials, attributing a strong and robust fibroblast accumulation at the implant site to PTFE and the lowest fibroblast accumulation to titanium. These findings are confirmed by the circular statistics of fibroblast migration. Interestingly, linear Kramers-Moyal drift coefficients have also been reported for swimming microorganisms attracted by a light source (Hill and Häder, 1997), indicating linear reorientation as a generic biological mechanism. *In vivo*, arriving fibroblasts remodel the tissue in the proximity of the biomaterial. To cover this long-term effect of macrophage-material interaction, we here propose a fibrous tissue model, including fibroblasts in a 3D collagen hydrogel matrix cultured under macrophage-material-conditioned medium. Tissue contraction, weight reduction, and deposition of extracellular matrix indicated a fibrotic process with a strong material dependency.

Our experimental design is aligned with the physiological microenvironment at the implant site. Dynamics of protein adsorption from blood fluid to biomaterial surface are resembled by the supplementation of FCS to the culture medium. Dependent on protein-surface, protein-protein, protein-water, and water-surface interactions, protein adsorption capacity from multi-complex biological fluids, like serum-supplemented cell culture medium, cannot be predicted from universal correlations (Vogler, 2012; Tejero et al., 2014). In our study, the measurement of growth factors in material-conditioned medium confirmed a strong material-dependency of protein adsorption. To identify macrophage-substrate effects on chemotaxis and tissue remodeling, material-conditioned blank medium was used as reference. With respect to material-conditioned control medium, a higher cellular net secretion, overlaying passive protein adsorption effects in macrophage-material-conditioned medium, was identified for chemotaxis and tissue remodeling. Interestingly, in addition to a material-dependent protein secretion, also a material-dependent protein consumption was observed, i.e., FGF was significantly decreased in the presence of macrophages on titanium. Particularly, with regard to material-induced cellular responses, single-cytokine measurements, here shown for FGF, PDGF, and TGF-β1, are not sufficient to allow ranking of biomaterials. Instead, using fibroblasts as a sensor of the net molecular secretion profile allows a better read out of cellular responses to biomaterials, here demonstrated for macrophage-material-mediated chemotaxis and tissue remodeling.

Our experiments on titanium surfaces revealed a higher macrophage-induced chemotactic activity, reflected by directed, forward-aligned fibroblast migration. These results are supported by the highest weight reduction ratio of the tissue model cultured under macrophage-titanium-conditioned medium compared to the titanium-medium control. In contrast to macrophage-induced chemotactic activity, the absolute weight of fibrous tissue related to initial weight remained high, leading to a relatively low collagen deposition observed in histology. Further insight is needed that reveals whether a higher cellular activity in response to biomaterials is favorable for the physiological healing process and might positively influence the end point of fibrous encapsulation. Macrophages cultured on PTFE surfaces stimulate a directed and forward-orientated migration of fibroblasts, however the alignment to the gradient was significantly lower compared to titanium. While the weight reduction ratio of fibrous tissue in comparison to blank medium control is moderate, the final weight related to the initial weight decreases greatly. This macrophage-PTFE-induced tissue contraction is strengthened by a high collagen fiber deposition.

State of the art *in vivo* models are based on histological evaluation, e.g., inflammatory infiltrates and matrix deposition. To our knowledge, there are no *in vivo* chemotaxis models

available, which continuously evaluate the biomaterials tested here. Our new *in vitro* test platform provides the advantage of allowing the study of the process of biomaterial-induced chemotaxis. *In vivo* studies have revealed a lower fibrous encapsulation and reactive inflammatory zone surrounding titanium implants compared to PTFE (Thomsen et al., 1986), copper (Suska et al., 2008), and stainless steel (Ungersböck et al., 1994). Formation of adherent fibrous tissue is reported for PTFE-aortic-patches in dogs (von Recum et al., 1978) as well as for vascular grafts in humans. Comparison of absolute weight reduction related to initial weight and collagen deposition with those *in vivo* studies, reveal a high consistency of developed fibrous tissue models to state-of-the-art scoring.

5 Conclusion

To date, the contributions of chemotaxis and tissue remodeling to the complex mechanisms of foreign body fibrous encapsulation could not be distinguished *in vitro*. We propose an *in vitro* multi-modular test platform that allows quantitative and qualitative evaluation of (I) material-induced chemotaxis and (II) tissue-remodeling by human fibroblasts. Significant differences in material dependency were found between the two processes, indicating that they are non-corresponding processes. Identification of processes with a strong material dependency enables informed decision making in biomaterial development.

References

Ahad, I. U., Butruk, B., Ayele, M. et al. (2015). Extreme ultraviolet (EUV) surface modification of polytetrafluoroethylene (PTFE) for control of biocompatibility. *Nucl Instrum Meth B 364*, 98-107. https://doi.org/10.1016/j.nimb.2015.08.093

Albini, A., Adelmann-Grill, B. C. and Müller, P. K. (1985). Fibroblast chemotaxis. *Coll Relat Res 5*, 283-296. https://doi.org/10.1016/S0174-173X(85)80018-2

Ambarus, C. A., Krausz, S., van Eijk, M. et al. (2012). Systematic validation of specific phenotypic markers for in vitro polarized human macrophages. *J Immunol Methods 375*, 196-206. https://doi.org/10.1016/j.jim.2011.10.013

Barron, L. and Wynn, T. A. (2011). Fibrosis is regulated by Th2 and Th17 responses and by dynamic interactions between fibroblasts and macrophages. *Am J Physiol Gastrointest Liver Physiol 300*, G723-728. https://doi.org/10.1152/ajpgi.00414.2010

Boilly, B., Vercoutter-Edouart, A. S., Hondermarck, H. et al. (2000). FGF signals for cell proliferation and migration through different pathways. *Cytokine Growth Factor Rev 11*, 295-302. https://doi.org/10.1016/S1359-6101(00)00014-9

Cheesborough, J. E., Liu, J., Hsu, D. et al. (2016). Prospective repair of ventral hernia working group type 3 and 4 abdominal wall defects with condensed polytetrafluoroethylene (MotifMESH) mesh. *Am J Surg 211*, 1-10. https://doi.org/10.1016/j.amjsurg.2015.03.033

Chen, S. Y., Lin, J. S., Lin, H. C. et al. (2015). Dependence of fibroblast infiltration in tumor stroma on type IV collagen-initiated integrin signal through induction of platelet-derived growth factor. *Biochim Biophys Acta 1853*, 929-939. https://doi.org/10.1016/j.bbamcr.2015.02.004

Coker, R. K., Laurent, G. J., Shahzeidi, S. et al. (1997). Transforming growth factors-beta 1, -beta 2, and -beta 3 stimulate fibroblast procollagen production in vitro but are differentially expressed during bleomycin-induced lung fibrosis. *Am J Pathol 150*, 981-991.

Franz, S., Rammelt, S., Scharnweber, D. et al. (2011). Immune responses to implants – a review of the implications for the design of immunomodulatory biomaterials. *Biomaterials 32*, 6692-6709. https://doi.org/10.1016/j.biomaterials.2011.05.078

Friedrich, R., Siegert, S., Peinke, J. et al. (2000). Extracting model equations from experimental data. *Physics Letters A 271*, 217-222. https://doi.org/10.1016/S0375-9601(00)00334-0

Grainger, D. W. (2013). All charged up about implanted biomaterials. *Nat Biotechnol 31*, 507-509. https://doi.org/10.1038/nbt.2600

Grant, M. B., Khaw, P. T., Schultz, G. S. et al. (1992). Effects of epidermal growth factor, fibroblast growth factor, and transforming growth factor-beta on corneal cell chemotaxis. *Invest Ophthalmol Vis Sci 33*, 3292-3301.

Heldin, C. H. and Westermark, B. (1999). Mechanism of action and in vivo role of platelet-derived growth factor. *Physiol Rev 79*, 1283-1316.

Hill, N. A. and Häder, D. P. (1997). A biased random walk model for the trajectories of swimming micro-organisms. *J Theor Biol 186*, 503-526. https://doi.org/10.1006/jtbi.1997.0421

Jaguin, M., Houlbert, N., Fardel, O. et al. (2013). Polarization profiles of human M-CSF-generated macrophages and comparison of M1-markers in classically activated macrophages from GM-CSF and M-CSF origin. *Cell Immunol 281*, 51-61. https://doi.org/10.1016/j.cellimm.2013.01.010

Kahlig, A., Hansmann, J., Groeber, F. et al. (2013). In silico approaches for the identification of optimal culture condition for tissue engineered bone substitutes. *Curr Anal Chem 9*, 16-28. https://doi.org/10.2174/157341113804486563

Mardia, K. V. (1972). *Statistics of Directional Data*. Academic Press. https://books.google.de/books?id=fG7c-yvRs38C

Mohammed, M. T., Khan, Z. A. and Siddiquee, A. N. (2014). Surface modifications of titanium materials for developing corrosion behavior in human body environment: A review. *Procedia Materials Science 6*, 1610-1618. https://doi.org/10.1016/j.mspro.2014.07.144

Möller, B., Terheyden, H., Açil, Y. et al. (2012). A comparison of biocompatibility and osseointegration of ceramic and titanium implants: An in vivo and in vitro study. *Int J Oral Maxillofac Surg 41*, 638-645. https://doi.org/10.1016/j.ijom.2012.02.004

Murray, L. A., Rosada, R., Moreira, A. P. et al. (2010). Serum amyloid P therapeutically attenuates murine bleomycin-induced pulmonary fibrosis via its effects on macrophages. *PLoS One 5*, e9683. https://doi.org/10.1371/journal.pone.0009683

Park, S., Park, M., Kim, B. H. et al. (2015). Acute suppression of TGF-ss with local, sustained release of tranilast against the formation of fibrous capsules around silicone implants.

J Control Release 200, 125-137. https://doi.org/10.1016/j.jconrel.2014.12.021

Pohlers, D., Brenmoehl, J., Loffler, I. et al. (2009). TGF-beta and fibrosis in different organs – molecular pathway imprints. *Biochim Biophys Acta 1792*, 746-756. https://doi.org/10.1016/j.bbadis.2009.06.004

Pudlas, M., Koch, S., Bolwien, C. et al. (2011). Raman spectroscopy: A noninvasive analysis tool for the discrimination of human skin cells. *Tissue Eng Part C Methods 17*, 1027-1040. https://doi.org/10.1089/ten.tec.2011.0082

Risken, H. (2012). *The Fokker-Planck Equation: Methods of Solution and Applications*. Berlin, Heidelberg: Springer. https://books.google.de/books?id=dXvpCAAAQBAJ

Rodriguez, A., Meyerson, H. and Anderson, J. M. (2009). Quantitative in vivo cytokine analysis at synthetic biomaterial implant sites. *J Biomed Mater Res A 89*, 152-159. https://doi.org/10.1002/Jbm.A.31939

Seppa, H., Grotendorst, G., Seppa, S. et al. (1982). Platelet-derived growth factor in chemotactic for fibroblasts. *J Cell Biol 92*, 584-588. https://doi.org/10.1083/jcb.92.2.584

Shreiber, D. I., Enever, P. A. J. and Tranquillo, R. T. (2001). Effects of PDGF-BB on rat dermal fibroblast behavior in mechanically stressed and unstressed collagen and fibrin gels. *Exp Cell Res 266*, 155-166. https://doi.org/10.1006/excr.2001.5208

Souza, J. C. M., Barbosa, S. L., Ariza, E. A. et al. (2015). How do titanium and Ti6Al4V corrode in fluoridated medium as found in the oral cavity? An in vitro study. *Mater Sci Eng C 47*, 384-393. https://doi.org/10.1016/j.msec.2014.11.055

Spiller, K. L., Nassiri, S., Witherel, C. E. et al. (2014). Sequential delivery of immunomodulatory cytokines to facilitate the M1-to-M2 transition of macrophages and enhance vascularization of bone scaffolds. *Biomaterials 37C*, 194-207. https://doi.org/10.1016/j.biomaterials.2014.10.017

Suska, F., Emanuelsson, L., Johansson, A. et al. (2008). Fibrous capsule formation around titanium and copper. *J Biomed Mater Res A 85*, 888-896. https://doi.org/10.1002/jbm.a.31575

Tejero, R., Anitua, E. and Orive, G. (2014). Toward the biomimetic implant surface: Biopolymers on titanium-based implants for bone regeneration. *Prog Polym Sci 39*, 1406-1447. https://doi.org/10.1016/j.progpolymsci.2014.01.001

Thomsen, P., Bjursten, L. M. and Ericson, L. E. (1986). Implants in the abdominal wall of the rat. *Scand J Plast Reconstr Surg 20*, 173-182. https://doi.org/10.3109/02844318609006316

Ungersböck, A., Perren, S. M. and Pohler, O. (1994). Comparison of the tissue reaction to implants made of a beta titanium alloy and pure titanium. Experimental study on rabbits. *J Mater Sci Mater Med 5*, 788-792. https://doi.org/10.1007/BF00213136

van Loon, S. L. M., Smits, A. I. P. M., Driessen-Mol, A. et al. (2013). The Immune Response in In Situ Tissue Engineering of Aortic Heart Valves. In E. Aikawa (ed.), *Calcific Aortic Valve Disease* (207-245). Rijeka, Croatia: InTech. https://doi.org/10.5772/54354

van Mourik, A. M., Daffertshofer, A. and Beek, P. J. (2006). Estimating Kramers-Moyal coefficients in short and non-stationary data sets. *Physics Letters A 351*, 13-17. https://doi.org/10.1016/j.physleta.2005.10.066

Verreck, F. A. W., de Boer, T., Langenberg, D. M. L. et al. (2006). Phenotypic and functional profiling of human proinflammatory type-1 and anti-inflammatory type-2 macrophages in response to microbial antigens and IFN-gamma- and CD40L-mediated costimulation. *J Leukoc Biol 79*, 285-293. https://doi.org/10.1189/jlb.0105015

Vogel, D. Y., Glim, J. E., Stavenuiter, A. W. et al. (2014). Human macrophage polarization in vitro: Maturation and activation methods compared. *Immunobiology 219*, 695-703. https://doi.org/10.1016/j.imbio.2014.05.002

Vogler, E. A. (2012). Protein adsorption in three dimensions. *Biomaterials 33*, 1201-1237. https://doi.org/10.1016/j.biomaterials.2011.10.059

von Recum, A. F., Imamura, H., Freed, P. S. et al. (1978). Biocompatibility tests of components of an implantable cardiac assist device. *J Biomed Mater Res 12*, 743-765. https://doi.org/10.1002/jbm.820120513

Zengel, P., Nguyen-Hoang, A., Schildhammer, C. et al. (2011). mu-Slide chemotaxis: A new chamber for long-term chemotaxis studies. *BMC Cell Biol 12*, 21. https://doi.org/10.1186/1471-2121-12-21

Conflict of interest

The authors declare no conflict of interest.

Acknowledgements

Our work was funded by the German Federal Ministry of Education and Research; program NanoMatFutur; grant agreement number 13N12971 – ETface.

Correspondence to

Jan Hansmann, Dr.-Ing.
University Hospital Wuerzburg
Roentgenring 11
97070 Wuerzburg, Germany
Phone: +49 931 3181209
e-mail: Jan.Hansmann@uni-wuerzburg.de